

LOCAL: Learning with Orientation Matrix to Infer Causal Structure from Time Series Data

Yue Cheng*
School of Software Engineering
Beijing Jiaotong University
Beijing, China
Pavel_cheng@foxmail.com

Jiajun Zhang*
School of Software Engineering
Beijing Jiaotong University
Beijing, China
jiajun0532@foxmail.com

Weiwei Xing†
School of Software Engineering
Beijing Jiaotong University
Beijing, China
wwxing@bjtu.edu.cn

Xiaoyu Guo
School of Software Engineering
Beijing Jiaotong University
Beijing, China
guoxiaoyu@bjtu.edu.cn

Xiaohui Gao
School of Automation
Northwestern Polytechnical
University
Xi'an, China
gaitxh@foxmail.com

ABSTRACT

Discovering the underlying *Directed Acyclic Graph* (DAG) from time series observational data is highly challenging due to the dynamic nature and complex nonlinear interactions between variables. Existing methods often struggle with inefficiency and the handling of high-dimensional data. To address these research gap, we propose LOCAL, a highly efficient, easy-to-implement, and constraint-free method for recovering dynamic causal structures. LOCAL is the first attempt to formulate a *quasi-maximum likelihood-based* score function for learning the dynamic DAG equivalent to the ground truth. On this basis, we propose two adaptive modules for enhancing the algebraic characterization of acyclicity with new capabilities: *Asymptotic Causal Mask Learning* (ACML) and *Dynamic Graph Parameter Learning* (DGPL). ACML generates causal masks using learnable priority vectors and the Gumbel-Sigmoid function, ensuring the creation of DAGs while optimizing computational efficiency. DGPL transforms causal learning into decomposed matrix products, capturing the dynamic causal structure of high-dimensional data and enhancing interpretability. Extensive experiments on synthetic and real-world datasets demonstrate that LOCAL significantly outperforms existing methods, and highlight LOCAL's potential as a robust and efficient method for dynamic causal discovery. Our code will be available soon.

CCS CONCEPTS

• **Computing methodologies** → Causal reasoning and diagnostics; Temporal reasoning.

KEYWORDS

Causal structure, Time series, Directed acyclic graph, Constraint free

1 INTRODUCTION

Exploration of the underlying causal generation process of dynamic systems is an important task [11, 19] for trustworthy machine learning. Unfortunately, it is unethical, impossible due to technical reasons, or expensive to conduct intervention experiments on the dynamic systems of certain domains [6, 25]. Another challenge is to infer about the structure which may be high dimensional and nonlinear. Some recent works [15, 18, 34, 37] have made significant efforts by employing *dynamic Bayesian networks* (DBNs) with observational and *interventional* data: *among dynamic systems, as illustrated in Figure 1. The variable x_i at timestep t is affected by which variables x_j at the same time step (instantaneous dependency) and which variables x_j at the previous timestep (lagged dependency)?* This question highlights the crucial roles of those algorithms in the interpretable performance of the trained models.

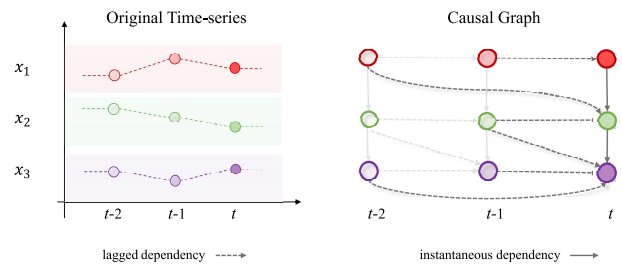


Figure 1: Illustration of instantaneous dependency (solid lines) and lagged dependency (dashed lines) dependencies in a DBN with $d = 3$ nodes and autoregression order $p = 2$. For clarity, we display edges that do not influence the variables at time t in a lighter shade.

In order to study the nonparametric DBN, DYNOTEARS [34] (i.e., a score-based approach to learning DBNs with a differentiable DAG constraint [43]) was proposed as a proxy to capture the learn

*Both authors contributed equally to this research.

†Corresponding author: Weiwei Xing.

the parents of child variables. However, in Section 4.2, our practical analysis shows that the DYNOTEARS algorithm and its extensions [15, 18, 37] adopting matrix exponential constraints require an extremely long time to optimize in high-dimensional dynamic systems, even if they smartly adopt interventional data to enhance the identifiability [26, 27]. Then, it is natural to need a proxy model that can fasterly infer dynamic causal structures in high-dimensional situations, which is also the main goal of our work.

Recently, much of the research on dynamic causal structure learning has concentrated on applying soft sparsity and DAG constraints. For instance, Golem [32] formulated a likelihood-based score function for handling the causality of thousands of nodes. Yu et al. [42] extended it for recovery dynamic causal structure. Concurrently, [16] verified the feasibility of further accelerating the learning of DAG based on this likelihood function both theoretically and experimentally. These approaches are aimed at enhancing flexibility and scalability in high-dimensional and circumventing rigid structural constraints.

Building on these insights, we propose a novel framework for Learning with Orientation matrix to infer CAusal structure from time series data, which we call **LOCAL**. We develop a quasi-maximum likelihood-based dynamic structure learning method with identifiability guarantee. Powered by this *quasi-maximum likelihood-based objective*, we propose to enhance the algebraic characterization of acyclicity with two adaptive modules for causal structure recovering task: 1) an Asymptotic Causal Mask Learning (ACML) module which leverages learnable priority vectors (\mathbf{p}) and the Gumbel-Sigmoid function to generate causal masks, ensuring the creation of directed acyclic graphs (DAGs) while optimizing computational efficiency; 2) a Dynamic Graph Parameter Learning (DGPL) module to transform causal learning into decomposed matrix products ($\mathbf{W} = \mathbf{E}_s \mathbf{E}_t^T$), effectively capturing the dynamic causal structure of high-dimensional data and enhancing interpretability. Those leads us can exploit faster gradient-based optimization, such as Adam [24], and GPU acceleration.

Contribution. The main contributions of this paper are as follows:

- To the best of our knowledge, LOCAL is the first attempt to formulate a quasi-maximum likelihood-based score function for learning the dynamic causal structure and shows that more robust and accurate.
- We proposed two adaptive modules, ACML and DGPL, which further liberate the matrix exponential operations required for causality.
- We conducted extensive experiments on several synthetic datasets and real-world benchmarks, which proved that LOCAL outperforms state-of-the-art by a significant margin.

2 RELATED WORK

2.1 Score-Based Objective for Causal Discovery

Learning causal structure from data using constraint and score-based techniques is a classic approach [29], but the major drawback is the computational inefficiency. Many recent works have made great efforts to promote computability and practicality: NOTEARS [43] employed a least squares objective to speed up the process, but

required augmented Lagrangian to satisfy hard DAG constraints. Based on this, DYNOTEARS [34] first tried to recover the causal structure of time series data. Golem [32] exploits the likelihood-based function to make the objective unconstrained. Those likelihood-based works, however, still struggled with the DAG constraint.

2.2 Constraint Free Causal Discovery

Many efforts have been made to emancipate constraints DAGs, focusing on designing more tractable optimization constraints [3, 7, 17, 40] on static data. In contrast to these approaches, Yu et al. [41] introduced NOCURL, which separated the topological ordering from the adjacency matrix, thereby eliminating the necessity to optimize the DAG constraint within the objective function. Inspired by NOCURL, a series of causal masks based on topological structures appeared [1, 28, 33]. For example, MCSL-MLP [33] sampled DAGs from a real matrix $U \in \mathbb{R}^{d \times d}$. BayesDAG [1] inherited NOCURL's grad matrix and directly sampled DAGs from the posterior of grad matrix $\mathbf{p}(u, v)$. By exploiting the temperature sigmoid function to $\mathbf{p}(u, v)$, COSMO [28] provides a fast implementation method when samples DAGs. However, DAG masks for the time domain datasets have rarely been studied.

2.3 Matrix Decomposed for Causal Discovery

The matrix decomposition approach is widely employed to address high-dimensional problems [10, 16, 28], with applications spanning large-scale parameter tuning [22], image restoration [9], and trajectory prediction [2]. While many of these works focus on learning intrinsic dimensionality to achieve efficient optimization in parameter space, VI-DP-DAG [8] adopts adjacency matrix decomposition \mathbf{W} as $\mathbf{W} = \mathbf{\Pi}^T \mathbf{U} \mathbf{\Pi}$, while LoRAM [14] integrates low-rank matrix factorization with sparsification mechanisms for continuous optimization of DAGs. Those works do not conduct an in-depth exploration of the physical meaning of the decomposition matrix, and the decomposition form is not concise enough.

3 LOCAL: LEARNING CAUSAL DISCOVERY FROM TIME SERIES DATA

3.1 Problem Definition

We target the causal discovery from a dynamic system. Consider multitudinous stationary time series that contains d causal univariate time series represented as $\mathcal{X} := [X_t^i] \in \mathbb{R}^{T \times d}$, where X_t^i is the recording of i -th component of X_t at time step t , our target is to simultaneously infer the *instantaneous dependency* $\mathbf{W}^i = \{\mathbf{W}^{i,j} : X_t^i \rightarrow X_t^j | i, j \in 1, \dots, d; i \neq j\}$ and the *lagged dependency* $\mathbf{A}^i = \{\mathbf{A}_k^{i,j} : X_{t-p}^j \rightarrow X_t^i | i, j \in 1, \dots, d; p \in \mathbb{Z}^+\}$ of X_t^i , from which we may recovery the dynamic causal structure. Following the practice in the dynamic causal structure discovery, we formulate the problem of learning a *dynamic Bayesian network (DBN)* that captures the dependencies in the X_t^i :

$$\begin{aligned} X_t &= X_t \mathbf{W} + \mathbf{Y} \mathbf{A} + \mathbf{N} \\ \text{s.t. } h(\mathbf{W}) &= 0 \end{aligned} \quad (1)$$

where $Y = [X_{t-1} \cdots |X_{t-p}] \in \mathbb{R}^{1 \times pd}$ is the p order time-lagged version of $X_t \in \mathbb{R}^{1 \times d}$, and $A = [A_1 | \cdots | A_p] \in \mathbb{R}^{pd \times d}$; N is the exogenous noise variables that are jointly Gaussian and independent; $h(W) = \text{Tr}(e^{W \circ W} - d)$ is a differentiable equality DAG constraint. Here, " \circ " denotes the Hadamard product of two matrices.

3.2 Quasi-Maximum Likelihood-Based Objective

Due to the hard acyclicity constraint [34], learning a DAG equivalent to the ground truth DAG through directly optimizing Eq. (1) is difficult. To circumvent this issue, we reformulate a score-based method to maximize the data quasi-likelihood of a dynamic linear Gaussian model.

The overall objective is defined as follows:

$$\begin{aligned} \min_{W, A} \mathcal{S}(W, A; X_t) &= \mathcal{L}(W, A; X_t) \\ + \lambda_1 h(W) &+ \lambda_2 (\mathcal{R}_{\text{sparse}}(A) + \mathcal{R}_{\text{sparse}}(W)) \end{aligned} \quad (2)$$

where $\mathcal{L}(W, A; X_t)$ is the quasi-maximum likelihood estimator (QMLE) of X , $\mathcal{R}_{\text{sparse}}$ is the penalty term encouraging sparsity, i.e. having fewer edges.

ASSUMPTION 1. Suppose N follows the multivariate normal distribution $\mathcal{N}(0, \sigma^2 I)$. Further assumes that the noise variances are equal, i.e. $\sigma_1^2 = \cdots = \sigma_d^2 = \sigma^2$. Let $X_t^{-i} = (X_t^j, j \neq i)^T$ denote the responses of all variables except for the i -th variable. Motivated by the least squares estimation (LSE) method [45], we have $\tilde{X}_t^i = E\{X_t^i | X_t^{-i}\} = \mu_i + \sum_{j \neq i} \alpha_{i,j} (X_t^j - \mu_j)$, where

$$\alpha_{ij} = \frac{(w_{ij} + w_{ji}) - \sum_k w_{ki} w_{kj}}{1 + \sum_k w_{ki}^2} \quad (3)$$

and $\mu_i = E(X_t^i)$.

Inspecting Eq. (3), we can find that for the i -th variable, the causal relationship are related to its first- and second-order parents or children, where the first-order parents or children are collected by $\{j : w_{ij} \neq 0 \text{ or } w_{ji} \neq 0\}$, and the second-order parents or children are collected by $\{j : \sum_k w_{ki} w_{kj} \neq 0\}$. Based on the conditional expectation and Eq. (3), we now derive that:

$$\begin{aligned} \tilde{X}_t^i - \mu_i &= (1 + \|\mathbf{W}_{\cdot i}\|^2)^{-1} (\mathbf{W}_{\cdot i} + \mathbf{W}_{\cdot i}^T - \mathbf{W}_{\cdot i}^T \mathbf{W}_{ii})(x_t - \mu) \\ &= (1 + \|\mathbf{W}_{\cdot i}\|^2)^{-1} \{(\mathbf{W}_{\cdot i} + \mathbf{W}_{\cdot i}^T - \mathbf{W}_{\cdot i}^T \mathbf{W}_{ii})(x_t - \mu) \\ &\quad - (X_t^i - \mu_i)\} + (X_t^i - \mu_i) \end{aligned} \quad (4)$$

By defining $D := \{I + \text{diag}(\mathbf{W}^T \mathbf{W})\}^{-1}$ and $S := I - \mathbf{W}$, we could verify the least squares objective function as

$$\frac{1}{n} \sum_{i=1}^d \|X_t^i S - Y^i A\|^2 = \frac{1}{n} \|\{X_t S - Y A\} D S^T\|^2 \quad (5)$$

Following the multivariate Gaussian distribution assumption, we now formulate a score-based method to maximize the data quasi-likelihood of the parameters in Eq. (2). Omitting additive constants, the log-likelihood is:

$$\begin{aligned} \mathcal{L}(W, A; X_t) &= \frac{1}{2} \log \sigma^2 - \log |\det(S)| \\ &\quad - \frac{1}{2} \frac{(X_t S - Y A)' (X_t S - Y A)}{\sigma^2} \end{aligned} \quad (6)$$

The QMLE in most common use is the maximizer of $\mathcal{L}(W, A; X_t)$. Solving $\frac{\partial \mathcal{L}}{\partial \sigma^2} = 0$ yields the estimate,

$$\hat{\sigma}^2 = \frac{1}{n} [X_t S - Y A]' [X_t S - Y A] \quad (7)$$

Maximization w.r.t. σ^2 gives $\hat{\sigma}^2 := \frac{1}{n} [X_t S - Y A]' [X_t S - Y A]$, the corresponding MLE is, again omitting additive constants,

$$\mathcal{L}(W, A; X_t) = \frac{d}{2} \log(\|X_t S - Y A\|^2) - \log |\det(S)| \quad (8)$$

Note that, the $\|X_t S - Y A\|^2$ term in Eq. (8) is the least squares objective, replace it with Eq. (5), we could verify the objective function as

$$\mathcal{L}(W, A; X_t) = \frac{d}{2} \log(\|\{X_t S - Y A\} D S^T\|^2) - \log |\det(S)| \quad (9)$$

3.3 Asymptotic Causal Mask Learning

Although QMLE can be statistically efficient, the computational cost could be expensive due to the matrix exponential operation of $h(\cdot)$ function [43]. Most recent work in causal structure learning deploys an alternative continuous DAG constraint $h(W)$ to characterize acyclic graphs. Although decoupling the causal structure into a causal mask and a real matrix may help to give more explanatory results for instantaneous causal effects, it means that the matrix needs to learn changes from $d \times d$ to $d \times (d + 1)$. To solve the issue, we propose an **Asymptotic Causal Mask Learning (ACML)** module to asymptotic infer the causal relationship from data automatically. The ACML module initializes a learnable priority vector $\mathbf{p} \in \mathbb{R}^d$, which is initialized as a vector with all elements set to 1, and a strictly positive threshold $\omega > 0$. Then the smooth orientation matrix of the strict partial order is the binary orientation matrix $\mathbf{M}_\omega(\mathbf{p})_{u,v} \in \{0, 1\}^{d \times d}$ such that:

$$\mathbf{M}_{\tau, \omega}(\mathbf{p})_{u,v} = \sigma_{\tau, \omega}(\mathbf{p}_v - \mathbf{p}_u) \quad (10)$$

where σ_ω can be formulated as the ω -centered Gumbel-Sigmoid:

$$\sigma_{\tau, \omega}(\mathbf{p}_v - \mathbf{p}_u) = \frac{\exp((\mathbf{p}_v - \mathbf{p}_u - \omega) + \hat{g})/\tau}{(\exp((\mathbf{p}_v - \mathbf{p}_u - \omega) + \hat{g})/\tau) + \exp(\hat{g}/\tau)} \quad (11)$$

where σ_ω is formulated as the ω -centered Gumbel-Sigmoid, \hat{g} and \tilde{g} are two independent Gumbel noises, and $\tau \in (0, \infty)$ is a temperature parameter. The threshold ω adjusts the midpoint of the sigmoid function and disrupts the symmetry when two variables have roughly equal priority. Finally, the ACML enhanced DBN can be formulated as:

$$X_t = X_t(W \circ \mathbf{M}_{\tau, \omega}(\mathbf{p})_{u,v}) + Y A + Z \quad (12)$$

3.4 Dynamic Graph Parameter Learning

Another problem lies in the existing dynamic causal structure models, which require directly learning $p + 1$ $d \times d$ -dimensional matrices. There are two main methods to capture dynamic causal effects: 1) Designing a complexity neural network, which specifically customizes a neural network with DAG constraint [18, 30]. 2) With the help of the Granger causal mechanism, [37] introduces the idea of Neural Granger's component network [38] to provide each variable design independent neural network. However, these approaches are quite unintuitive. Overly complex network design or component Neural Granger [12, 44] methods are overparameterized, but most works in practice only exploit the first-layer weights of the network to characterize causal effects, which increases the optimization cost and has to adopt a second-order optimizer L-BFGS-B. Besides, over-parameterization methods are prone to overfitting when dealing with unsupervised problems such as causal structure discovery, leading to considerable biases in the causal structure.

To solve the issue, we propose a *Dynamic Graph Parameter Learning (DGPL)* module to infer the dynamic causal graphs from observed data and interventional data automatically. The DGPL module first randomly initializes 2 learnable dynamic node embedding dictionaries $E_{so} \in \mathbb{R}^{(p+1) \times d \times k}$, $E_{to} \in \mathbb{R}^{(p+1) \times d \times k}$ for all nodes, where each row of E_{so} represents the source embedding of a node, each row of E_{to} represents the target embedding of a node. Then, we can infer the causal structure between each pair of nodes by multiplying E_{so} and E_{to} :

$$\begin{aligned} W &= E_{so}(t)E_{to}^T(t) \\ A &= [E_{so}(t-1)E_{to}^T(t-1)] \cdots [E_{so}(t-p)E_{to}^T(t-p)] \end{aligned} \quad (13)$$

where W is instantaneous dependency, A is lagged dependency. During training, E_{so} and E_{to} will be updated automatically to learn the causal structure among different variables. Compared with the CNN-based work in [37], the DGPL module is simpler and the learned embedding matrices have better interpretability (see Section 4.6 for more details). Finally, the DGPL enhanced DBN can be formulated as:

$$X_t = X_t(E_{so}(t)E_{to}^T(t) \circ M_{\tau,\omega}(\mathbf{p})_{u,v}) + Y A_{so} \circ A_{to} + Z \quad (14)$$

where $A_{so} = [E_{so}(t-1)] \cdots [E_{so}(t-p)] \in \mathbb{R}^{pd \times k}$ is the lagged source embedding matrix, and $A_{to} = [E_{to}(t-1)] \cdots [E_{to}(t-p)] \in \mathbb{R}^{pd \times k}$ is the lagged target embedding matrix, " \circ " means that each entry matrix in the two matrices is multiplied.

3.5 Nonlinear Form and Model Training

3.5.1 Nonlinear Form. In practice, the interactions among variables can be highly nonlinear, increasing the difficulty in modeling. To alleviate this issue, we adopt *1D Convolutional Neural Networks (CNN)*, a classical nonlinear model for temporal data, to capture nonlinear interactions. We replace the 3D convolutional kernel with two consecutive kernels, which are estimates of E_{so} and E_{to} . Formally, a convolutional kernel in a 1D CNN is 3D tensor $\mathcal{W} \in \mathbb{R}^{K \times d \times d}$, where $K = p + 1$ is the number of convolution kernels and d is the input feature dimension. Let $X_{t-p:t} \in \mathbb{R}^{B \times T \times d}$

be the input temporal data, then the output is defined as:

$$\begin{aligned} X_t &= \mathcal{W}^{p+1} * (\mathcal{W}^p * \cdots * (\mathcal{W}^1 * X_{t-p:t})) = \theta^T X_{t-p:t} \\ \text{s.t. } \mathcal{W}^c &= E_S^c(E_t^c)^T, \forall c \in \{1, \dots, p+1\} \end{aligned} \quad (15)$$

where \mathcal{W}^c represents the c -th filter, E_{so}^c is to learn whether the variable X_j is the root cause of other variables in the causal structure, E_{to}^c is to learn whether the variable X_j is affected by other root causes, while E_{so} and E_{to} are denoted as collections of E_{so}^c and E_{to}^c . "*" is the convolution operation.

Similar to [37], The first layer of each CNN is a 1D convolution layer with $p + 1$ kernels, stride equal to 1, and no padding, where the last kernels $p + 1$ represent instantaneous dependency. Finally, the CNN enhanced **LOCAL (LOCAL-CNN)** can be formulated as:

$$\begin{aligned} \hat{X}_t &= CNN(X_{t-p:t}; \theta^{(q)}) \\ \text{s.t. } \mathcal{W}^{p+1(q)} &:= \mathcal{W}^{p+1(q)} \circ M_{\tau,\omega}(\mathbf{p}^{(q)})_{u,v} \end{aligned} \quad (16)$$

3.5.2 Model Training. In this part, we combine the ACML and DGPL modules with QMLE, then the overall loss function $\mathcal{S}(W, A; X_t)$ becomes:

$$\begin{aligned} \mathcal{S}(W, A; X_t) &= \mathcal{S}(E_{so}, E_{to}, \mathbf{p}; X_t) \\ &= \frac{d}{2} \log(\|DS^T\{SX_t - YA\}\|^2) - \log|\det(S)| \\ &\quad + \lambda_2(\mathcal{R}_{sparse}(A) + \mathcal{R}_{sparse}(W)) \end{aligned} \quad (17)$$

where $S := I - E_{so}(t)E_{to}^T(t) \circ M_{\tau,\omega}(\mathbf{p})_{u,v}$, $A := A_{so} \circ A_{to}$, $W := E_{so}(t)E_{to}^T(t) \circ M_{\tau,\omega}(\mathbf{p})_{u,v}$.

For the nonlinear form, the overall objective becomes:

$$\begin{aligned} \mathcal{S}(W, A; X_t) &= \mathcal{S}(E_{so}, E_{to}, \mathbf{p}; X_t) \\ &= \frac{d}{2} \log(\|DS^T\{X_t - CNN(X_{t-p:t}; \theta^{(q)})\}\|^2) \\ &\quad - \log|\det(S)| + \lambda_2(\mathcal{R}_{sparse}(A) + \mathcal{R}_{sparse}(W)) \end{aligned} \quad (18)$$

4 EXPERIMENTS

In this section, we conduct extensive experiments to answer the following research questions:

- **RQ1:** As a framework based on temporal causal discovery, can **LOCAL** accurately recover causal structures according to the DBN from Eq. (1)?
- **RQ2:** Can **LOCAL** accurately recover causal structures based on complex nonlinear fMRI dataset?
- **RQ3:** Can causal structures discovered by **LOCAL** align with expert knowledge on real-world dataset?
- **RQ4:** How do the key designs and parameters in **LOCAL** affect performance?
- **RQ5:** What are the physical meanings of source embedding and target embedding matrices?

4.1 Experimental Setup

This section provides an overview of the datasets, hyper-parameters setting, evaluation metrics, and compared baselines.

4.1.1 Data Descriptions. The performance of **LOCAL** is evaluated on three datasets. The first dataset is a synthetic dataset created to test **LOCAL**'s ability to recover the underlying causal structures.

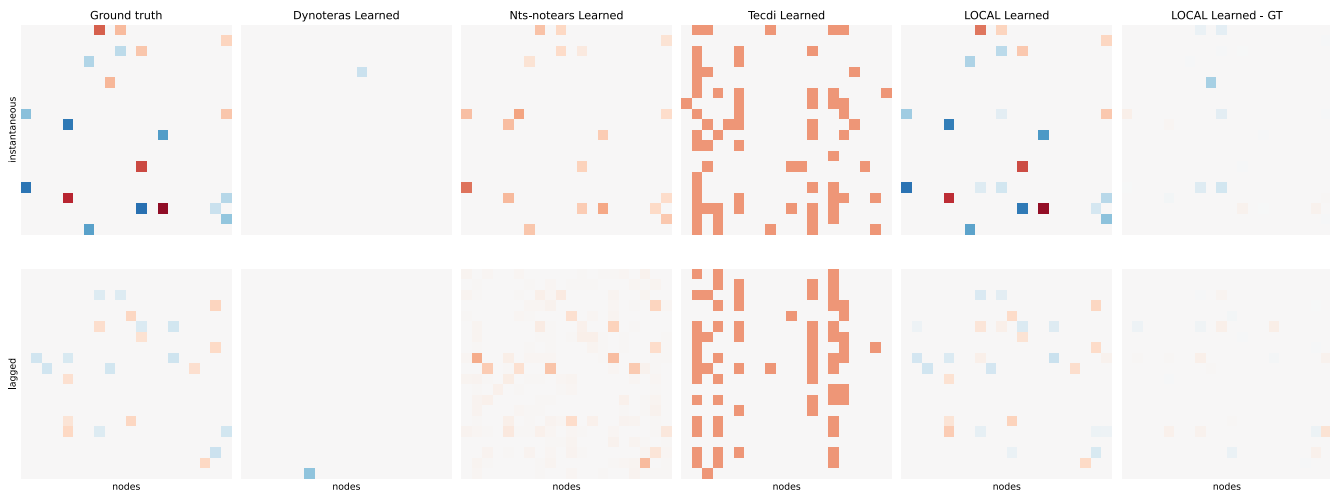


Figure 2: A show case of the result on synthetic data with $d = 20$ nodes, $T = 1000$ timesteps, $p = 1$ lagged order. Our algorithm recovers weights that are close to the ground truth.

We produce temporal data through a two-step process: **1)** sample contemporaneous and time-lagged matrices using the *Erdős-Rényi* scheme. Populate the contemporaneous matrix \mathbf{W} with elements uniformly distributed over the ranges $[-2.0, -0.5] \cup [0.5, 2.0]$. For the time-lagged matrices A_k , sample elements from $[-1.0\alpha, -0.25\alpha] \cup [0.25\alpha, 2.0\alpha]$, where $\alpha = 1/\eta^k$, $\eta \leq 1$, $k = 1, \dots, p$; **2)** generate time series data that adheres to the sampled weighted graph according to the specified equation Eq. (1). The second, NetSim [36], is an fMRI dataset designed to facilitate the study of evolving challenges in brain networks. NetSim comprises 28 datasets, from which we select 17 with the same sequence length. Each selected dataset consists of 50 independent time series recordings, capturing the activity of 5-15 nodes over 200 time steps. The third, CausalTime [12], is a real-world dataset that contains 3 types of benchmark time series from weather, traffic, and healthcare scenarios respectively. The total length of the dataset is 8760 (Air Quality Index subset), 52116 (Traffic subset), and 40000 (Medical subset); the number of nodes is 36 (Air Quality Index subset), 20 (Traffic subset), and 20 (Medical subset).

4.1.2 Hyper-parameter Settings. In this study, each DGPL module includes a source embedding matrix $E_{so} \in \mathbb{R}^{(p+1) \times d \times k}$ and a target embedding matrix $E_{to} \in \mathbb{R}^{(p+1) \times d \times k}$. For the ACML module, we employ a \mathbf{p} vector to represent the priority relationship between nodes and exploit the ω -centered Gumbel sigmoid function to sample the orientation matrix derived. The translation parameter ω is carefully set to 0.01 to ensure optimal performance. The dimension k of the embedding matrix in DGPL is determined as $\frac{2}{5} \times d$. Under this configuration, the parameter amount of the embedding matrix is marginally smaller than $d \times d$, ensuring efficient representation of the data while mitigating computational complexity. Additionally, the value of the l_1 penalty term λ_2 is set to 0.01 to regulate the sparsity of the learned causal structures. For

synthetic datasets, the batch size is set to 16, while for real-world datasets, a batch size of 64 is utilized. Training and inference were performed on an NVIDIA GeForce RTX 3090 machine, with an average training time of 20 minutes.

4.1.3 Evaluation Metrics. We evaluate the performance of our proposed method for learning causal graphs using three main metrics: **1) True Positive Rate (TPR)**, which measures the proportion of actual positives that are correctly identified by the model; **2) Structural Hamming Distance (SHD)**, which counts the number of discrepancies (such as reversed, missing, or redundant edges) between two DAGs; **3) F1 score**, which represents the harmonic mean of precision and recall, effectively balancing the two in the evaluation process. Given that the number of potential non-causal relationships vastly outnumbers true causal relationships in real datasets, we utilize the Area Under the Precision-Recall Curve (**AUPRC**) and the Area Under the ROC Curve (**AUROC**) to evaluate **LOCAL**'s effectiveness in identifying genuine and significant causal relationships.

4.1.4 Compared Methods. To answer the first question (RQ1), we compare our **LOCAL** method with the following popular baselines. Table 1 summarizes the difference between previous methods and **LOCAL**.

- **DYNOTEARS** [34]: DYNOTEARS is a scalable method for learning the structure of DBN from time-series data to efficiently estimate both contemporaneous and time-lagged relationships among variables.
- **NTS-NOTEARS** [37]: NTS-NOTEARS is an extension of the nonlinear CNN version of DYNOTEARS and integrates prior knowledge to improve accuracy.
- **TECDI** [26]: TECDI incorporates intervention data into time series analysis to effectively reveal nonlinear temporal causal relationships, and is the current SOTA model.

Table 1: Difference between existing methods and LOCAL.

Method	DYNO	NTS	TEDCI	LOCAL
Optimizer	L-BFGS-B	L-BFGS-B	SGD	Adam
Constraint Free	✓	✓	✓	✓
Augmented Lagrangian	✓	✓	✓	✗
Non-linearity	✗	✓	✓	✓
Mini-batch	✗	✗	✓	✓
Contemporaneous	✓	✓	✓	✓
Time-lagged	✓	✓	✓	✓

To answer the second question (RQ2), we additionally compare **LOCAL** with several competitive methods as follows:

- NGC [38]: NGC is a neural Granger causal structure learning method that leverages an LSTM or MLP to predict the future and conduct causal discovery based on input weights.
- PCMCI [35]: PCMCI is a causal structure learning algorithm based on non-linear independence tests of time series.

To answer the third question (RQ3), we further compare **LOCAL** with recent or representative causal discovery methods that were directly reproduced by Cheng [12].

To verify the effectiveness of the quasi-likelihood objective, DGPL module, and ACML module (RQ4), we introduce three variants of **LOCAL** as follows:

- **LOCAL w/o ACML**. It removes the ACML module with a causal constraint.
- **LOCAL w/o DGPL**. It removes the DGPL module with a $d \times d$ causal matrix.
- **LOCAL w/o QMLE**. It removes the quasi-maximum likelihood estimator (QMLE) with the LSE.

4.2 On Synthetic Datasets (RQ1)

To answer RQ1, we conduct experiments across three simulated datasets, each respectively containing {5, 10, 20, 50, 100} nodes. Each node is accompanied by $p = 1$ autoregression terms. Correspondingly, each dataset includes {5, 10, 20, 50, 100} distinct intervention targets, with each target focused on a different node. Figure 2 shows the learned instantaneous matrix W and lagged matrix A on dataset 1 under different algorithms. It can be observed that compared with others, the causal structure learned by **LOCAL** is almost consistent with the ground truth.

Table 2: Performance on Synthetic Data Under TPR, SHD and F1 score with lower dimension ($d \leq 20$).

Methods	d=5, lag=1			d=10, lag=1			d=20, lag=1		
	TPR ↑	SHD ↓	F1 score ↑	TPR ↑	SHD ↓	F1 score ↑	TPR ↑	SHD ↓	F1 score ↑
DYNO [34]	0.53±0.19	2.33±0.94	0.68±0.15	0.07±0.09	4.67±0.07	0.11±0.16	0.10±0.04	18.00±0.82	0.18±0.07
NTS-NO [37]	0.93±0.09	0.33±0.47	0.92±0.05	0.93±0.09	0.67±0.94	0.91±0.13	0.80±0.11	17.67±11.44	0.79±0.14
TECDI [26]	0.93±0.25	4.00±0.82	0.33±0.24	0.33±0.34	5.67±3.80	0.32±0.34	0.20±0.13	66.00±1.09	0.09±0.05
LOCAL	0.23±0.09	1.00±0.82	0.90±0.08	0.87±0.09	1.00±0.82	0.87±0.11	0.82±0.02	4.32±1.25	0.82±0.09
LOCAL-CNN	1.00±0.00	0.33±0.47	0.97±0.04	0.93±0.09	0.33±0.47	0.96±0.05	0.95±0.00	3.67±1.70	0.89±0.04
DYNO [34]	0.07±0.00	3.33±1.25	0.00±0.00	0.00±0.00	7.33±1.25	0.00±0.00	0.35±0.04	17.33±1.19	0.05±0.04
NTS-NO [37]	1.00±0.00	33.67±1.09	0.39±0.05	1.00±0.00	113.00±11.36	0.26±0.04	1.00±0.00	546.67±15.06	0.11±0.03
TECDI [26]	0.29±0.15	2.67±0.94	0.43±0.17	0.52±0.20	3.67±2.69	0.62±0.19	0.39±0.06	53.33±11.90	0.19±0.03
LOCAL	0.88±0.09	3.67±1.70	0.67±0.08	1.00±0.00	2.67±1.09	0.89±0.11	0.99±0.02	15.67±6.02	0.69±0.13
LOCAL-CNN	1.00±0.00	0.33±0.47	0.97±0.04	1.00±0.00	1.00±0.82	0.95±0.04	1.00±0.00	8.00±2.79	0.82±0.10

Across the synthetic datasets, we conduct three runs of both the baseline methods and **LOCAL**, averaging the results to obtain final performance indicators. The main results of causal structure

Table 3: Performance on Synthetic Data Under TPR, SHD and F1 score with higher dimension ($d \geq 50$).

Methods	d=50, lag=1			d=100, lag=1		
	TPR ↑	SHD ↓	F1 score ↑	TPR ↑	SHD ↓	F1 score ↑
DYNO [34]	0.00±0.00	50.00±0.00	0.00±0.00	0.00±0.00	100.00±0.00	0.00±0.00
NTS-NO [37]	0.77±0.17	17.67±11.44	0.79±0.14	0.56±0.13	72.67±10.87	0.56±0.10
TECDI [26]	0.28±0.00	184.00±0.00	0.12±0.00	0.22±0.00	187.00±0.00	0.12±0.00
LOCAL	0.93±0.06	22.33±21.82	0.81±0.15	0.91±0.03	47.00±11.86	0.78±0.05
LOCAL-CNN	0.89±0.04	26.00±11.78	0.77±0.08	0.93±0.01	40.67±8.18	0.81±0.03
DYNO [34]	1.00±0.00	1272.33±1.25	0.04±0.01	1.00±0.00	5048.00±0.82	0.02±0.00
NTS-NO [37]	1.00±0.00	3510.33±544.48	0.05±0.01	1.00±0.00	14462.00±425.94	0.02±0.00
TECDI [26]	0.22±0.00	187.00±0.00	0.12±0.00	1.00±0.00	5049.00±0.00	0.02±0.00
LOCAL	0.93±0.04	77.00±31.63	0.57±0.10	0.97±0.00	234.33±22.51	0.46±0.01
LOCAL-CNN	0.99±0.01	53.67±12.55	0.66±0.07	0.99±0.01	143.00±6.38	0.59±0.02

learning are shown in Figure 3. To further exploit the effectiveness of **LOCAL** under the DBN datasets, we also report TPR, SHD, and F1 score results in Table 2 and Table 3. It is evident that when the variable dimension is high (i.e., $d > 50$), **LOCAL** significantly outperforms the baseline model across all three evaluation metrics (TPR, SHD, and F1 score). Notably, **LOCAL** exhibits a notable improvement of 226.19% in TPR. This superior performance can be attributed to the adaptability of the **LOCAL** decomposition strategy to high-dimensional data, coupled with the inherently sparse and low-rank structure of the simulation data. Regarding computational efficiency, as depicted in Figure 4, **LOCAL** demonstrates an average time savings of 97.83% compared to other score-based algorithms. This efficiency gain stems from **LOCAL**'s avoidance of matrix exponential operations and its utilization of a first-order optimizer. These computational advantages contribute to the practical scalability of **LOCAL** in analyzing large-scale datasets.

4.3 On NetSim Datasets (RQ2)

To answer RQ2, we conduct the NetSim experiment, which depicts a dataset characterized by high complexity and nonlinear attributes. We show AUROC and AUPRC results in Table 4. Notably, **LOCAL** demonstrates significant superiority over the baseline method in both linear and nonlinear scenarios, showcasing an average increase of 4.11% in AUPRC (12.33% for **LOCAL-CNN**) and an average increase of 9.59% in AUROC (12.33% for **LOCAL-CNN**) while saving 66.63% of time. It is worth mentioning that, due to the ground truth of NetSim not adhering to the low-rank assumption, we slightly increase the embedding dimension to $k = 20$ for **LOCAL-CNN**. This adjustment enables **LOCAL-CNN** to effectively capture the intricate relationships within the dataset, contributing to its enhanced performance compared to the baseline method.

4.4 On CausalTime Datasets (RQ3)

To answer RQ3, we employ a real-world dataset CausalTime to evaluate the performance of **LOCAL**. A detailed comparison will be presented in Table 5. We can observe that: (1) Among all the compared methods, **LOCAL** performs best in the Traffic subset and second-best in Medical, which demonstrates the effectiveness of the proposed method. (2) Our **LOCAL** achieves the average best performance, which is attributed to the helpful role of explicitly instantaneous and lagged causality information. (3) The linear implementation of **LOCAL** is more suitable for the CausalTime dataset

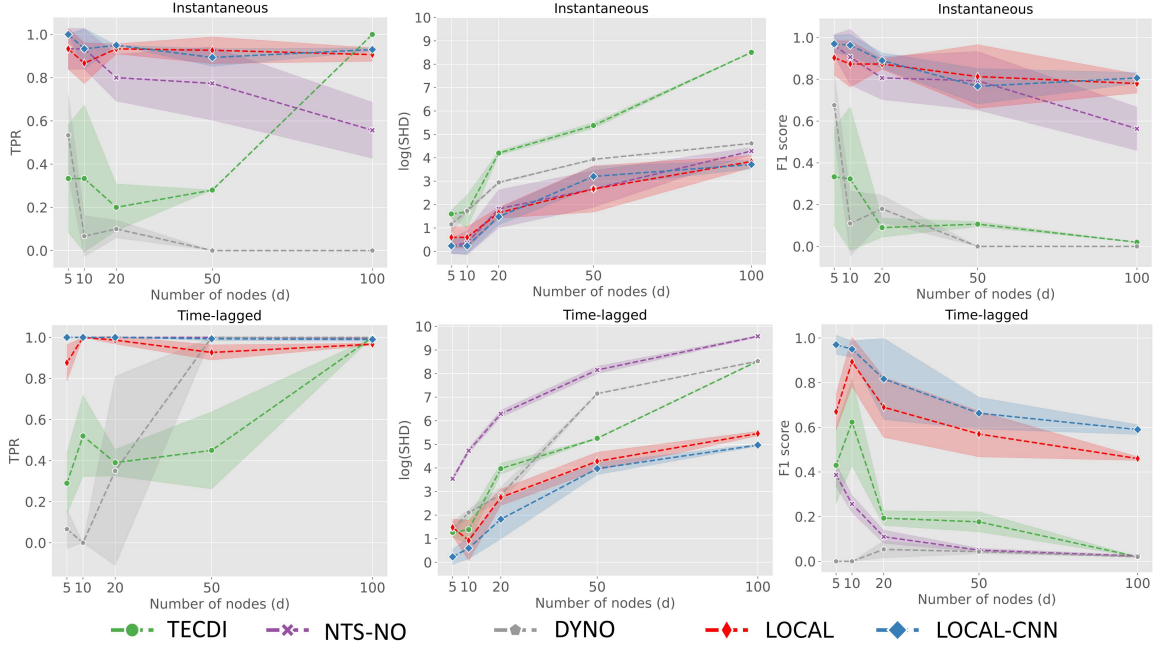


Figure 3: TPR, FDR, and F1 scores for different nodes $d = \{5, 10, 20, 50, 100\}$. Each row contains results for three different metrics of intra-slice and inter-slice graphs.

Table 4: Performance on NetSim Data Under AUROC and AUPRC.

Dataset	AUPRC							AUROC						
	NGC [38]	PCMCi [35]	DYNO [34]	NTS-NO [37]	TECDI [26]	LOCAL	LOCAL-CNN	NGC [38]	PCMCi [35]	DYNO [34]	NTS-NO [37]	TECDI [26]	LOCAL	LOCAL-CNN
Sim1	0.42±0.15	0.39±0.09	0.41±0.08	0.41±0.10	0.67±0.03	<u>0.79±0.03</u>	0.89±0.01	0.65±0.12	0.64±0.12	0.73±0.08	0.64±0.12	0.67±0.03	0.85±0.06	<u>0.78±0.05</u>
Sim2	0.29±0.11	0.29±0.11	0.33±0.12	0.24±0.11	<u>0.79±0.02</u>	0.71±0.01	0.87±0.02	0.68±0.11	0.69±0.12	0.81±0.08	0.50±0.10	0.79±0.05	<u>0.87±0.01</u>	0.87±0.02
Sim3	0.26±0.12	0.26±0.12	0.32±0.13	0.16±0.15	<u>0.73±0.05</u>	0.57±0.01	0.76±0.00	0.72±0.12	0.73±0.13	0.85±0.07	0.51±0.08	0.73±0.06	<u>0.85±0.01</u>	0.89±0.02
Sim8	0.40±0.14	0.36±0.10	0.36±0.08	0.42±0.08	0.58±0.04	<u>0.80±0.01</u>	0.88±0.02	0.62±0.12	0.61±0.11	0.66±0.10	0.49±0.10	0.58±0.03	<u>0.75±0.01</u>	0.94±0.01
Sim10	0.42±0.16	0.40±0.12	0.38±0.10	0.46±0.06	0.71±0.06	<u>0.86±0.03</u>	0.90±0.01	0.65±0.16	0.66±0.15	0.69±0.12	0.58±0.11	0.71±0.06	<u>0.83±0.00</u>	0.78±0.01
Sim11	0.25±0.08	0.25±0.07	0.26±0.04	0.21±0.10	0.74±0.04	0.53±0.01	<u>0.68±0.02</u>	0.67±0.09	0.68±0.10	0.77±0.04	0.47±0.10	0.74±0.08	0.83±0.03	<u>0.77±0.02</u>
Sim12	0.28±0.11	0.29±0.11	0.36±0.08	0.21±0.05	<u>0.79±0.05</u>	0.70±0.02	0.87±0.01	0.68±0.12	0.70±0.13	0.83±0.05	0.47±0.11	0.79±0.04	<u>0.87±0.05</u>	0.88±0.02
Sim13	0.47±0.11	0.47±0.10	0.47±0.05	0.53±0.07	<u>0.68±0.07</u>	0.77±0.02	<u>0.74±0.02</u>	0.59±0.12	0.59±0.12	0.66±0.08	0.43±0.10	0.68±0.07	<u>0.76±0.00</u>	0.82±0.02
Sim14	0.41±0.13	0.38±0.09	0.41±0.08	0.42±0.08	0.67±0.03	<u>0.72±0.05</u>	0.92±0.04	0.65±0.13	0.64±0.11	0.74±0.08	0.39±0.12	0.67±0.10	<u>0.76±0.01</u>	0.86±0.02
Sim15	0.47±0.20	0.41±0.10	0.38±0.07	0.42±0.08	0.72±0.05	<u>0.80±0.03</u>	0.86±0.02	0.68±0.16	0.66±0.12	0.68±0.07	0.46±0.08	0.72±0.05	<u>0.80±0.01</u>	0.79±0.02
Sim16	0.46±0.10	0.44±0.06	0.44±0.05	0.50±0.06	0.64±0.06	<u>0.73±0.00</u>	0.91±0.02	0.59±0.11	0.59±0.09	0.64±0.07	0.45±0.15	0.64±0.11	<u>0.73±0.02</u>	0.93±0.03
Sim17	0.40±0.19	0.35±0.10	0.39±0.09	0.22±0.12	<u>0.86±0.05</u>	0.76±0.03	0.90±0.01	0.77±0.13	0.76±0.13	<u>0.87±0.05</u>	0.52±0.12	0.86±0.05	0.83±0.01	0.87±0.02
Sim18	0.42±0.16	0.40±0.11	0.42±0.07	0.41±0.06	0.68±0.08	<u>0.75±0.01</u>	0.89±0.02	0.65±0.16	0.64±0.14	0.74±0.08	0.45±0.12	0.68±0.01	0.82±0.03	<u>0.80±0.00</u>
Sim21	0.41±0.14	0.38±0.09	0.42±0.08	0.43±0.09	0.68±0.05	<u>0.79±0.01</u>	0.88±0.02	0.64±0.13	0.63±0.12	0.74±0.08	0.44±0.08	0.68±0.02	<u>0.80±0.04</u>	0.83±0.03
Sim22	0.35±0.09	0.37±0.08	0.38±0.06	0.45±0.06	0.83±0.02	0.69±0.03	<u>0.80±0.01</u>	0.58±0.13	0.61±0.12	0.66±0.07	0.48±0.09	0.83±0.10	<u>0.76±0.01</u>	0.72±0.02
Sim23	0.45±0.20	0.41±0.21	0.35±0.06	0.41±0.05	0.78±0.05	0.64±0.01	<u>0.64±0.00</u>	0.67±0.15	0.65±0.11	0.64±0.06	0.43±0.07	0.78±0.01	<u>0.75±0.02</u>	0.67±0.03
Sim24	0.34±0.11	0.35±0.11	0.31±0.07	0.47±0.08	0.79±0.05	<u>0.65±0.02</u>	<u>0.57±0.02</u>	0.55±0.13	0.57±0.12	0.53±0.01	0.47±0.09	0.79±0.06	0.69±0.04	<u>0.71±0.01</u>
Average	0.38±0.12	0.36±0.10	0.38±0.08	0.37±0.10	<u>0.73±0.04</u>	0.72±0.02	0.82±0.02	0.65±0.12	0.65±0.12	0.72±0.08	0.46±0.07	0.73±0.04	<u>0.80±0.02</u>	0.82±0.02

than the nonlinear version, one possible reason is that the causal relationship between the data appears linear.

4.5 Ablation and Parameter Study (RQ4)

To answer RQ4, we compare LOCAL with three ablation methods. Initially, as presented in Table 6, causal relationships are extracted solely from a $d \times d$ matrix. Subsequently, we enhance the basic low-rank structure by incorporating interventional data and an Asymptotic Causal Mask, leading to substantial performance improvements. Finally, the optimal performance is achieved when all

components are integrated into the LOCAL model. This progressive integration of components is illustrated in Figure 5, highlighting the incremental enhancements in performance as each component is added to the model.

Figure 6 illustrates that to achieve at least 90% accuracy (using TPR as the evaluation metric), the minimum dimension k increases as the rank-to- d ratio rises, and is approximately proportional to the true rank of the graph structure. This trend may be linked to the inherent data structure: lower matrix ranks often correspond to graphs with significant centralization. As k increases, graph complexity also rises, necessitating a higher dimension to capture the

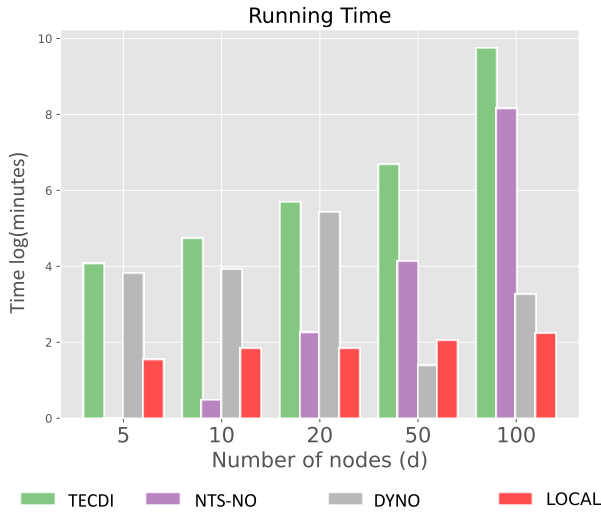


Figure 4: The average running time over 5 datasets measured in minutes with $d = \{5, 10, 20, 50, 100\}$, $T = 1000$ timesteps, $p = 1$ lagged order. The heights of bars are on a logarithmic scale.

Table 5: Performance on CausalTime Data Under AUROC and AUPRC.

Methods	AUROC			AUPRC		
	AQI	Traffic	Medical	AQI	Traffic	Medical
GC [21]	0.45±0.04	0.42±0.03	0.57±0.03	0.63±0.02	0.28±0.00	0.42±0.03
SVAR [37]	0.62±0.04	0.63±0.00	0.71±0.02	0.79±0.02	0.58±0.00	0.68±0.04
NTS-NO [37]	0.57±0.02	0.63±0.03	0.71±0.02	0.71±0.02	0.58±0.05	0.46±0.02
PCMCI [35]	0.53±0.07	0.54±0.07	0.70±0.01	0.67±0.04	0.35±0.06	0.51±0.02
Rhino [20]	0.67±0.10	0.63±0.02	0.65±0.02	0.76±0.08	0.38±0.01	0.49±0.03
CUTS [13]	0.60±0.00	0.62±0.02	0.37±0.03	0.51±0.04	0.15±0.02	0.15±0.00
CUTS+ [11]	0.89 ±0.02	0.62±0.07	0.82 ±0.02	0.80 ±0.08	0.64 ±0.12	0.55±0.13
NGC [38]	0.72±0.01	0.60±0.01	0.57±0.01	0.72±0.01	0.36±0.05	0.46±0.01
NGM [4]	0.67±0.02	0.47±0.01	0.56±0.02	0.48±0.02	0.28±0.01	0.47±0.02
LCCM [5]	<u>0.86</u> ±0.07	0.55±0.03	0.80±0.02	0.93 ±0.02	0.59±0.05	0.76 ±0.02
eSRU [23]	0.83±0.03	0.60±0.02	0.76±0.04	0.72±0.03	0.49±0.03	<u>0.74</u> ±0.06
SCGL [39]	0.49±0.05	0.59±0.06	0.50±0.02	0.36±0.03	0.45±0.03	0.48 ±0.02
TCDF [31]	0.41±0.02	0.50±0.00	0.63±0.04	0.65±0.01	0.36±0.00	0.55±0.03
LOCAL	0.85±0.02	0.89 ±0.01	<u>0.81</u> ±0.03	0.67±0.00	0.68 ±0.01	0.73±0.03
LOCAL-CNN	0.85±0.01	<u>0.83</u> ±0.00	<u>0.74</u> ±0.02	0.70±0.01	0.62±0.01	0.67±0.01

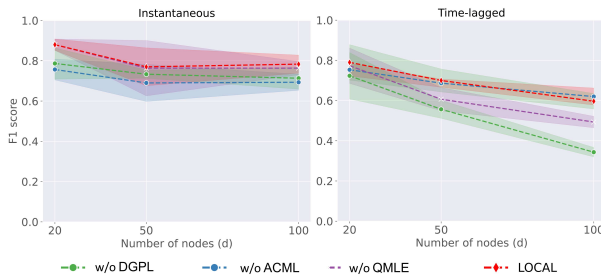


Figure 5: Illustration of ablation study on Synthetic data with $d = \{20, 50, 100\}$ nodes, $T = 1000$ timestep, p -order = 1

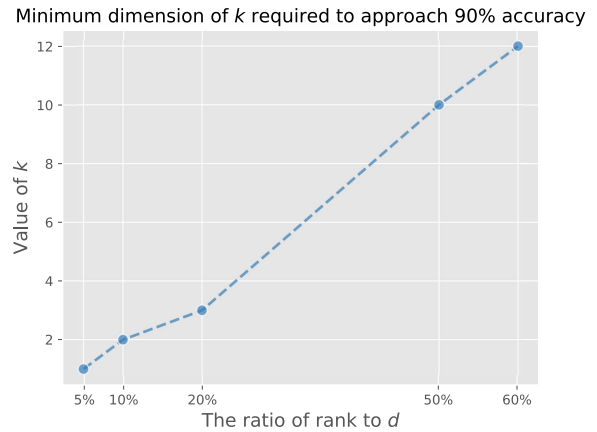


Figure 6: The minimum dimension k required for synthetic data with order = 1 to achieve 90% accuracy under different ranks (5%, 10%, 20%, 50%, 60%) for $d = 20$ nodes and $T = 1000$ time steps.

data’s complexity and diversity effectively. This finding aids in selecting an optimal k to maintain accuracy. When the rank is unknown, choosing k to be slightly less than 0.5 times d can balance performance and computational efficiency.

4.6 Embedding Matrices Visualization (RQ5)

To answer RQ5, this section visualizes the learned source embedding and target embedding in a synthetic dataset with $d = 5$. We illustrate the ground truth instantaneous causal graph, source embedding $E_{so}(t)$, and target embedding $E_{to}(t)$ in Figure 7. As we can see, the $d \times d$ -dimensional causal matrix W is decomposed into E_{so} and E_{to} , where each row of the source embedding E_{so} corresponds to the variable embedding result in W as parents. Each row of target embedding E_{to} corresponds to the variable embedding result of children. This is exactly why we named it source and target embedding.

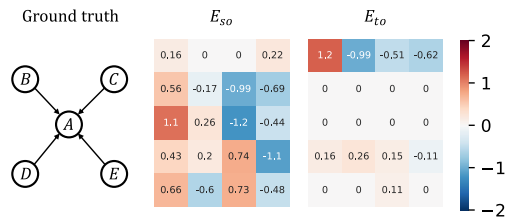


Figure 7: Illustration of node source embedding matrix and target embedding matrix in a DBN with $d = 5$ nodes.

5 CONCLUSION

In this work, we introduce an easy-to-implement variant to the dynamic causal discovery family, LOCAL, particularly tailored for

Table 6: Ablation Study on Synthetic Data with $d = \{20, 50, 100\}$ Nodes, $T = 1000$ Timestep, p -order = 1

Dataset	d=20			d=50			d=100		
	tpr \uparrow	shd \downarrow	f1 \uparrow	tpr \uparrow	shd \downarrow	f1 \uparrow	tpr \uparrow	shd \downarrow	f1 \uparrow
w/o DGPL	0.95/1.00	6.33/12.33	0.84/0.77	0.86/1.00	42.00/151.33	0.66/0.43	0.91/1.00	58.67/565.33	0.75/0.26
w/o ACML	0.75/0.90	18.67/21.00	0.58/0.61	0.92/0.88	52.00/74.67	0.63/0.58	0.87/0.89	66.00/150.00	0.70/0.54
w/o QMLE	0.95/1.00	6.00/9.67	0.84/0.82	0.84/0.91	53.00/116.67	0.60/0.47	0.89/0.96	62.33/237.33	0.73/0.44
LOCAL	0.93/0.99	4.33/15.67	0.87/0.69	0.93/0.93	22.33/77.00	0.81/0.57	0.91/0.97	47.00/234.33	0.78/0.46

capturing nonlinear, high-dimension dynamic systems rapidly. Specifically, it estimates causal structure and connection strength through a quasi-maximum likelihood-based score function, Asymptotic Causal Mask Learning (ACML) and Dynamic Graph Parameter Learning (DGPL) modules respectively. We evaluate our approach on both synthetic and public benchmark datasets, LOCAL has presented advantages over previous state-of-the-art approaches. In the future, we aim to design additional neural network architectures for LOCAL, including attention-based methods.

ACKNOWLEDGMENTS

This work was supported by Beijing Natural Science Foundation under Grant (No.XXXX).

REFERENCES

- Yashas Annadani, Nick Pawlowski, Joel Jennings, Stefan Bauer, Cheng Zhang, and Wenbo Gong. 2023. BayesDAG: Gradient-Based Posterior Inference for Causal Discovery. In *Advances in Neural Information Processing Systems*. 1738–1763.
- Inhwan Bae, Jean Oh, and Hae-Gon Jeon. 2023. EigenTrajectory: Low-Rank Descriptors for Multi-Modal Trajectory Forecasting. In *Proceedings of the IEEE/CVF International Conference on Computer Vision (ICCV)*. 10017–10029.
- Kevin Bello, Bryon Aragam, and Pradeep Ravikumar. 2022. DAGMA: Learning DAGs via M-matrices and a Log-Determinant Acyclicity Characterization. In *Advances in Neural Information Processing Systems*, S. Koyejo, S. Mohamed, A. Agarwal, D. Belgrave, K. Cho, and A. Oh (Eds.). 8226–8239.
- Alexis Bellot, Kim Branson, and Mihaela van der Schaar. 2022. Neural graphical modelling in continuous-time: consistency guarantees and algorithms. In *International Conference on Learning Representations*. <https://openreview.net/forum?id=SsHBkfeRF9L>
- Edward De Brouwer, Adam Arany, Jaak Simm, and Yves Moreau. 2021. Latent Convergent Cross Mapping. In *International Conference on Learning Representations*. <https://openreview.net/forum?id=4TSiOTkKe5P>
- Wei Cai, Fuli Feng, Qifan Wang, Tian Yang, Zhenguang Liu, and Congfu Xu. 2023. A Causal View for Item-level Effect of Recommendation on User Preference. In *Proceedings of the Sixteenth ACM International Conference on Web Search and Data Mining (WSDM '23)*. Association for Computing Machinery, 240–248.
- Yunfeng Cai, Xu Li, Mingting Sun, and Ping Li. 2023. Recovering Linear Causal Models with Latent Variables via Cholesky Factorization of Covariance Matrix. arXiv:2311.00674 [stat.ML]
- Bertrand Charpentier, Simon Kibler, and Stephan Günnemann. 2022. Differentiable DAG Sampling. In *International Conference on Learning Representations*.
- Lin Chen, Xue Jiang, Xingzhao Liu, and Martin Haardt. 2022. Reweighted Low-Rank Factorization With Deep Prior for Image Restoration. *IEEE Transactions on Signal Processing* 70 (2022), 3514–3529.
- Siya Chen, HaoTian Wu, and Guang Jin. 2024. Causal structure learning for high-dimensional non-stationary time series. *Knowledge-Based Systems* 295 (2024), 111868.
- Yuxiao Cheng, Lianglong Li, Tingxiang Xiao, Zongren Li, Jinli Suo, Kunlun He, and Qionghai Dai. 2024. CUTS+: High-Dimensional Causal Discovery from Irregular Time-Series. *Proceedings of the AAAI Conference on Artificial Intelligence* 38, 10 (Mar. 2024), 11525–11533.
- Yuxiao Cheng, Ziqian Wang, Tingxiang Xiao, Qin Zhong, Jinli Suo, and Kunlun He. 2024. CausalTime: Realistically Generated Time-series for Benchmarking of Causal Discovery. In *The Twelfth International Conference on Learning Representations*. <https://openreview.net/forum?id=iad1yyGme>
- Yuxiao Cheng, Runzhao Yang, Tingxiang Xiao, Zongren Li, Jinli Suo, Kunlun He, and Qionghai Dai. 2023. CUTS: Neural Causal Discovery from Irregular Time-Series Data. In *The Eleventh International Conference on Learning Representations*. <https://openreview.net/forum?id=UG8bQcD3Emv>
- Shuyu Dong and Michèle Sebag. 2023. From Graphs to DAGs: A Low-Complexity Model and a Scalable Algorithm. In *Machine Learning and Knowledge Discovery in Databases*. 107–122.
- Shaohua Fan, Shuyang Zhang, Xiao Wang, and Chuan Shi. 2023. Directed Acyclic Graph Structure Learning from Dynamic Graphs. In *the AAAI Conference on Artificial Intelligence*. 7512–7521.
- Zhuangyan Fang, Shengyu Zhu, Jiji Zhang, Yue Liu, Zhitang Chen, and Yangbo He. 2024. On Low-Rank Directed Acyclic Graphs and Causal Structure Learning. *IEEE Transactions on Neural Networks and Learning Systems* 35, 4 (2024), 4924–4937.
- Muhammad Hasan Ferdous, Uzma Hasan, and Md Osman Gani. 2023. CDANs: Temporal Causal Discovery from Autocorrelated and Non-Stationary Time Series Data. In *Proceedings of the 8th Machine Learning for Healthcare Conference*. 186–207.
- Tian Gao, Debarun Bhattacharjya, Elliot Nelson, Miao Liu, and Yue Yu. 2022. IDYNO: Learning Nonparametric DAGs from Interventional Dynamic Data. In *the International Conference on Machine Learning*. PMLR, 6988–7001.
- Chang Gong, Di Yao, Lei Zhang, Sheng Chen, Wenbin Li, Yueyang Su, and Jingping Bi. 2024. CausalMMM: Learning Causal Structure for Marketing Mix Modeling. In *Proceedings of the 17th ACM International Conference on Web Search and Data Mining*. 238–246.
- Wenbo Gong, Joel Jennings, Cheng Zhang, and Nick Pawlowski. 2023. Rhino: Deep Causal Temporal Relationship Learning with History-dependent Noise. In *The Eleventh International Conference on Learning Representations*. https://openreview.net/forum?id=i_1rbq8yFWC
- Clive WJ Granger. 1969. Investigating causal relations by econometric models and cross-spectral methods. *Econometrica: journal of the Econometric Society* (1969), 424–438.
- Edward J Hu, yelong shen, Phillip Wallis, Zeyuan Allen-Zhu, Yuanzhi Li, Shean Wang, Lu Wang, and Weizhu Chen. 2022. LoRA: Low-Rank Adaptation of Large Language Models. In *the International Conference on Learning Representations*.
- Saurabh Khanna and Vincent Y. F. Tan. 2020. Economy Statistical Recurrent Units For Inferring Nonlinear Granger Causality. In *International Conference on Learning Representations*. <https://openreview.net/forum?id=SyxV9ANFDH>
- Diederik Kingma and Jimmy Ba. 2015. Adam: A Method for Stochastic Optimization. In *the International Conference on Learning Representations*.
- Adam Li, Amin Jaber, and Elias Bareinboim. 2023. Causal discovery from observational and interventional data across multiple environments. In *Advances in Neural Information Processing Systems*. 16942–16956.
- Peiwen Li, Yuan Meng, Xin Wang, Fang Shen, Yue Li, Jialong Wang, and Wenwu Zhu. 2023. Causal Discovery in Temporal Domain from Interventional Data. In *the International Conference on Information and Knowledge Management*. 4074–4078.
- Peiwen Li, Xin Wang, Zeyang Zhang, Yuan Meng, Fang Shen, Yue Li, Jialong Wang, Yang Li, and Wenwu Zhu. 2024. LLM-Enhanced Causal Discovery in Temporal Domain from Interventional Data. arXiv:2404.14786 [cs.AI]
- Ricardo Massidda, Francesco Landolfi, Martina Cinquini, and Davide Bacciu. 2024. Constraint-Free Structure Learning with Smooth Acyclic Orientations. In *the International Conference on Learning Representations*.
- David Maxwell Chickering and David Heckerman. 1997. Efficient approximations for the marginal likelihood of Bayesian networks with hidden variables. *Machine learning* 29 (1997), 181–212.
- Panagiotis Misiakos, Chris Wendler, and Markus Püschel. 2023. Learning DAGs from Data with Few Root Causes. In *Advances in Neural Information Processing Systems*, A. Oh, T. Naumann, A. Globerson, K. Saenko, M. Hardt, and S. Levine (Eds.). 16865–16888.

- [31] Meike Nauta, Doina Bucur, and Christin Seifert. 2019. Causal Discovery with Attention-Based Convolutional Neural Networks. *Machine Learning and Knowledge Extraction* 1, 1 (2019), 312–340. <https://doi.org/10.3390/make1010019>
- [32] Ignavier Ng, AmirEmad Ghassami, and Kun Zhang. 2020. On the Role of Sparsity and DAG Constraints for Learning Linear DAGs. In *Advances in Neural Information Processing Systems*, Vol. 33. 17943–17954.
- [33] Ignavier Ng, Shengyu Zhu, Zhuangyan Fang, Haoyang Li, Zhitang Chen, and Jun Wang. 2022. Masked gradient-based causal structure learning. In *the SIAM International Conference on Data Mining*. 424–432.
- [34] Roxana Pamfil, Nisara Sriwattanaworachai, Shaan Desai, Philip Pilgerstorfer, Konstantinos Georgatzis, Paul Beaumont, and Bryon Aragam. 2020. DYNOTEARS: Structure Learning from Time-Series Data. In *International Conference on Artificial Intelligence and Statistics*. PMLR, 1595–1605.
- [35] Jonas Peters, Dominik Janzing, and Bernhard Schölkopf. 2013. Causal Inference on Time Series using Restricted Structural Equation Models. In *Advances in Neural Information Processing Systems*, Vol. 26.
- [36] Stephen M Smith, Karla L Miller, Gholamreza Salimi-Khorshidi, Matthew Webster, Christian F Beckmann, Thomas E Nichols, Joseph D Ramsey, and Mark W Woolrich. 2011. Network modelling methods for FMRI. *Neuroimage* 54, 2 (2011), 875–891.
- [37] Xiangyu Sun, Oliver Schulte, Guiliang Liu, and Pascal Poupart. 2023. NTS-NOTEARS: Learning Nonparametric DBNs With Prior Knowledge. In *International Conference on Artificial Intelligence and Statistics*. PMLR, 1942–1964.
- [38] Alex Tank, Ian Covert, Nicholas Foti, Ali Shojaie, and Emily B Fox. 2021. Neural granger causality. *IEEE Transactions on Pattern Analysis and Machine Intelligence* 44, 8 (2021), 4267–4279.
- [39] Chenxiao Xu, Hao Huang, and Shinjae Yoo. 2019. Scalable Causal Graph Learning through a Deep Neural Network. In *Proceedings of the 28th ACM International Conference on Information and Knowledge Management (Beijing, China) (CIKM '19)*. 1853–1862.
- [40] Yue Yu, Jie Chen, Tian Gao, and Mo Yu. 2019. DAG-GNN: DAG Structure Learning with Graph Neural Networks. In *Proceedings of the 36th International Conference on Machine Learning*. 7154–7163.
- [41] Yue Yu, Tian Gao, Naiyu Yin, and Qiang Ji. 2021. DAGs with No Curl: An Efficient DAG Structure Learning Approach. In *the International Conference on Machine Learning*, Vol. 139. PMLR, 12156–12166.
- [42] Yue Yu, Xuan Kan, Hejie Cui, Ran Xu, Yujia Zheng, Xiangchen Song, Yanqiao Zhu, Kun Zhang, Raziieh Nabi, Ying Guo, Chao Zhang, and Carl Yang. 2023. Deep Dag Learning of Effective Brain Connectivity for FMRI Analysis. In *2023 IEEE 20th International Symposium on Biomedical Imaging (ISBI)*. 1–5.
- [43] Xun Zheng, Bryon Aragam, Pradeep K Ravikumar, and Eric P Xing. 2018. DAGs with NO TEARS: Continuous Optimization for Structure Learning. In *Advances in Neural Information Processing Systems*.
- [44] Wanqi Zhou, Shuanghao Bai, Shujian Yu, Qibin Zhao, and Badong Chen. 2024. Jacobian Regularizer-based Neural Granger Causality. In *Forty-first International Conference on Machine Learning*. <https://openreview.net/forum?id=FG5hjRBtpm>
- [45] Xuening Zhu, Danyang Huang, Rui Pan, and Hansheng Wang. 2020. Multivariate spatial autoregressive model for large scale social networks. *Journal of Econometrics* 215, 2 (2020), 591–606.